

# Emulating computationally expensive dynamical simulators using Gaussian processes

Hossein Mohammadi\*, Peter Challenor, and Marc Goodfellow

College of Engineering, Mathematics and Physical Sciences,  
University of Exeter, UK

## Abstract

A Gaussian process (GP)-based methodology is proposed to emulate computationally expensive dynamical computer models or simulators. The method relies on emulating the short-time numerical flow map of the model. The flow map returns the solution of a dynamic system at an arbitrary time for a given initial condition. The prediction of the flow map is performed via a GP whose kernel is estimated using random Fourier features. This gives a distribution over the flow map such that each realisation serves as an approximation to the flow map. A realisation is then employed in an iterative manner to perform one-step ahead predictions and forecast the whole time series. Repeating this procedure with multiple draws from the emulated flow map provides a probability distribution over the time series. The mean and variance of that distribution are used as the model output prediction and a measure of the associated uncertainty, respectively. The proposed method is used to emulate several dynamic non-linear simulators including the well-known Lorenz attractor and van der Pol oscillator. The results show that our approach has a high prediction performance in emulating such systems with an accurate representation of the prediction uncertainty.

**Keywords:** Dynamic system; Emulation; Gaussian process; Random Fourier features

## 1 Introduction

The problem of predicting the output of complex computer codes occurs frequently in many applications. Such simulators are computationally intensive, and hence the number of simulation runs is limited by our budget for computation. One way to overcome this problem is to create a surrogate of

---

\*Corresponding author: h.mohammadi@exeter.ac.uk

the complex computer code. Surrogate models are statistical representation of the true model relying on a limited number of simulation runs and are cheap-to-evaluate. Among broad types of surrogate models, Gaussian process (GP) emulators [38] have become the gold standard for the design and analysis of computer experiments [12, 39, 40]. This is due to their statistical properties such as the flexibility and computational tractability. GPs offer a probabilistic paradigm for modelling unknown functions such that their prediction is equipped with an estimation of the associated uncertainty, see Section 2 for further detail.

An important class of computer codes are those with a time series output known as *dynamical simulators*. They simulate the evolution of a physical process over time and are commonly used in many applications e.g. in cardiology to study the dynamics of electrical activity of the cardiac membrane [33], and in climate science to model the Atlantic thermohaline circulation [48]. Another example is the Hindmarsh-Rose (HR) model [24] which simulates the dynamics of a single neuron. More details about the HR model and its emulation are given in Section 5.3. Emulating dynamic computer codes is an active field of research and has been tackled via different statistical and machine learning approaches, see e.g. [7, 10, 11, 34, 37]. The focus of this paper is on emulating deterministic dynamical simulators relying on a set of ordinary differential equations (ODE) using GPs.

One may consider the problem of emulating dynamical simulators as a special case of the multi-output GPs [1, 14, 20] with a temporal dependency between the outputs. However, the size of the output dimension in dynamical models is usually too high to be treated by multi-output GPs. To tackle this issue one can first apply techniques such as principal component analysis [23, 26] or wavelet decomposition [4, 17] to reduce the output dimensionality. The pitfall is that we lose some information by not keeping all the components. Another approach is proposed in [27] to account for time using an extra input parameter. This method increases the computational complexity and is reported to be inefficient [13, 32]. The idea of forecasting the time series through iterative one-step ahead predictions is developed in [5, 13]. This method relies on emulating the transition function from one time point to the next, under the assumption that the model output at time  $t$  depends only on the output at time  $t - 1$ , i.e. the Markov property. The work is continued in [34] by considering the input uncertainty in each step of the one-step ahead prediction paradigm. The method needs to estimate the correlation between emulators of state variables, and hence is not efficient if the problem dimensions, i.e. the number of variables in the ODE, are large.

This paper presents a novel approach for emulating non-linear dynamic simulators that are computationally intensive. The method is based on approximating the numerical flow map over a short period of time by a GP whose kernel is approximated via random Fourier features (RFF), see Section 3.1. The flow map can be regarded as the solution trajectory of a

dynamical system that starts from a given initial condition and represents the evolution of the system with time. This way of emulating the flow map creates a probability distribution over it such that any realisation from that distribution is an approximation to the flow map. Drawing multiple realisations from the emulated flow map to perform on-step ahead predictions gives a distribution over the time series. The mean and variance of that distribution serve as the time series forecast and the associated uncertainty, respectively. The results show that our method has a high predictive performance in emulating dynamic simulators and yields an accurate representation of the uncertainty associated with the model output prediction. In the following, a brief summary of dynamic systems is presented.

**Dynamical system** A dynamical system represents the evolution of a phenomenon over time according to a fixed mathematical rule. It is expressed in terms of differential equations whose (time-varying) variables are called *state variables* and describe the state of the system at any given time. The space that consists of all possible values of the state variables is called the *state (phase) space*. The *vector field* is the time derivative of the state variables given by

$$v : \mathcal{X} \mapsto \mathcal{X}, \quad \frac{d}{dt} \mathbf{x}(t) = v(\mathbf{x}(t)), \quad (1)$$

in which  $\mathbf{x}(t) = (x_1(t), \dots, x_d(t))^\top \in \mathcal{X} \subset \mathbb{R}^d$  is the state vector at time  $t \in \mathbb{R}$  [43]. We assume that the system is autonomous meaning that the associated vector field does not depend on time explicitly. The *flow map* is a function that maps the initial condition  $\mathbf{x}_0$ , i.e. the state of the system at  $t_0$ , to the state at the next time step  $t_1 = t_0 + \Delta t$  [16]:

$$F : \mathcal{X} \times \mathbb{R} \mapsto \mathcal{X}, \quad (\mathbf{x}_0, \Delta t) \xrightarrow{F} \mathbf{x}(t_0 + \Delta t), \quad (2)$$

The flow map can be interpreted as a trajectory traced out in the state space from  $\mathbf{x}_0$  to  $\mathbf{x}(t_1)$ . In this work, we assume that the time step  $\Delta t$  is fixed, and hence the flow map is a function of  $\mathbf{x}_0$  only.

## 2 Gaussian process emulators

Our aim is to build statistical representations of the flow map based on GPs to enable efficient construction of trajectories with quantified uncertainty. The potential benefits of this approach are shown in [34]. Before explaining the advances in the current manuscript, we introduce GP emulators.

Let  $f(\mathbf{x}), \mathbf{x} \in \mathcal{X}$ , be the function we wish to emulate via the stochastic Gaussian process  $Y(\mathbf{x})$  given by

$$Y(\mathbf{x}) = \mu_0(\mathbf{x}) + Z(\mathbf{x}). \quad (3)$$

Here,  $\mu_0 : \mathcal{X} \mapsto \mathbb{R}$  is called the *trend function* which is deterministic and can take any functional form. In this work, a linear trend function is considered

$$\mu_0(\mathbf{x}) = \mathbf{q}(\mathbf{x})^\top \boldsymbol{\beta}, \quad (4)$$

such that  $\mathbf{q}(\mathbf{x}) = [q_1(\mathbf{x}), \dots, q_r(\mathbf{x})]^\top$  is a vector of basis functions (regression functions) and  $\boldsymbol{\beta} = [\beta_1, \dots, \beta_r]^\top$  comprises the corresponding coefficients. The second component in Equation (3),  $Z(\mathbf{x})$ , is a centred (or zero mean) GP and is fully determined by its kernel or correlation function  $k$  defined as

$$k : \mathcal{X} \times \mathcal{X} \mapsto \mathbb{R}, \quad \sigma_0^2 k(\mathbf{x}, \mathbf{x}') = \text{Cov}(Z(\mathbf{x}), Z(\mathbf{x}')). \quad (5)$$

The scalar  $\sigma_0^2$  is called the *signal (process) variance* and regulates the scale of the amplitude of  $Z(\mathbf{x})$ . A kernel is called *stationary (shift invariant)* if it depends only on the difference between its inputs:  $k(\mathbf{x}, \mathbf{x}') = k(\mathbf{x} - \mathbf{x}')$ . One of the most common stationary correlation functions is the squared exponential (SE) kernel given by

$$k_{SE}(\mathbf{x}, \mathbf{x}') = \exp\left(-0.5(\mathbf{x} - \mathbf{x}')^\top \boldsymbol{\Delta}^{-1}(\mathbf{x} - \mathbf{x}')\right), \quad (6)$$

where  $\boldsymbol{\Delta}$  is a diagonal matrix [38]. Its diagonal elements  $\delta_i, i = 1, \dots, d$ , represent the *correlation length-scale* in dimension  $i$ . Often, the length-scales and other parameters such as  $\sigma_0^2$  and  $\boldsymbol{\beta}$  are unknown and need to be estimated. In this work, these parameters are estimated by maximum likelihood, see Appendix A.

Let  $\mathcal{D} = \{\mathbf{X}, \mathbf{y}\}$  denote the training data set in which  $\mathbf{X} = (\mathbf{x}^1, \dots, \mathbf{x}^n)^\top$  is the design matrix. The rows of  $\mathbf{X}$  are  $n$  cites in the  $d$ -dimensional input space with the corresponding outputs  $\mathbf{y} = (f(\mathbf{x}^1), \dots, f(\mathbf{x}^n))^\top$ . For our purpose,  $\mathbf{x}^1, \dots, \mathbf{x}^n$  represent samples taken from the state space and are used to emulate the flow map, see Section 4. The predictive distribution of  $Y(\mathbf{x})$  is obtained by conditioning  $Z(\mathbf{x})$  on  $\mathcal{D}$ . This has a Gaussian distribution whose mean and variance are

$$\mu_n(\mathbf{x}) = \mu_0(\mathbf{x}) + \mathbf{k}(\mathbf{x})^\top \mathbf{K}^{-1}(\mathbf{y} - \boldsymbol{\mu}), \quad (7)$$

$$\sigma_n^2(\mathbf{x}) = \sigma_0^2 \left(1 - \mathbf{k}(\mathbf{x})^\top \mathbf{K}^{-1} \mathbf{k}(\mathbf{x})\right), \quad (8)$$

in which  $\boldsymbol{\mu} = \mu_0(\mathbf{X})$  and  $\mathbf{k}(\mathbf{x}) = [k(\mathbf{x}^1, \mathbf{x}), \dots, k(\mathbf{x}^n, \mathbf{x})]^\top$ . Also,  $\mathbf{K}$  is an  $n \times n$  correlation matrix whose  $ij$ -th element is  $\mathbf{K}_{ij} = k(\mathbf{x}^i, \mathbf{x}^j), \forall \mathbf{x}^i, \mathbf{x}^j \in \mathbf{X}$ . It is worth mentioning that the computational complexity of inverting the correlation matrix  $\mathbf{K}$  is of order  $\mathcal{O}(n^3)$ .

GPs can be regarded from a different perspective called the *weight space view* in which  $Z(\mathbf{x})$  is represented by a weighted sum of (possibly infinite) basis functions as

$$Z(\mathbf{x}) = \boldsymbol{\phi}(\mathbf{x})^\top \mathbf{w}. \quad (9)$$

Here,  $\mathbf{w}$  is the weight vector which is assumed to be a Gaussian random variable and  $\phi(\mathbf{x})$  is called the *feature map*; it transfers the input space  $\mathcal{X}$  to the reproducing kernel Hilbert space  $\mathcal{H}$  [2]. In this framework, the stochastic process  $Y(\mathbf{x})$  is given by  $Y(\mathbf{x}) = \mu_0(\mathbf{x}) + \phi(\mathbf{x})^\top \mathbf{w}$  whose predictive distribution is obtained by conditioning the weights on the training data, i.e.  $p(\mathbf{w} | \mathcal{D})$ . The predictive mean and variance of  $Y(\mathbf{x})$  take the following forms [38, 44]

$$\mu_n(\mathbf{x}) = \mu_0(\mathbf{x}) + \phi(\mathbf{x})^\top (\Phi \Phi^\top)^{-1} \Phi (\mathbf{y} - \boldsymbol{\mu}), \quad (10)$$

$$\sigma_n^2(\mathbf{x}) = \sigma_0^2 \phi(\mathbf{x})^\top (\Phi \Phi^\top)^{-1} \phi(\mathbf{x}), \quad (11)$$

in which  $\Phi = [\phi(\mathbf{x}^1), \dots, \phi(\mathbf{x}^n)]$  is the aggregation of columns of  $\phi(\mathbf{x})$  for all points in the training set [38]. Note that the computational complexity of  $(\Phi \Phi^\top)^{-1}$  is a function of the dimensionality of the feature map and not the number of data points  $n$ .

### 3 Kernel approximation

This section provides the material necessary for approximating a kernel with random Fourier features. A GP whose kernel is approximated this way offers a probability distribution over its predictive mean and allows us to draw realisations from the predictive mean distribution. This idea is used in Section 4 to emulate dynamical simulators where multiple realisations from the emulated flow map are employed iteratively to perform one-step ahead predictions. We start the discussion by random Fourier features first developed by Rahimi and Recht [36].

#### 3.1 Random Fourier features

Random Fourier features (RFF) provides an effective way to approximate stationary kernels relying on the Bochner's theorem [6]. According to this theorem, the stationary kernel  $k$  can be expressed by

$$k(\mathbf{x}, \mathbf{x}') = \int e^{-i\boldsymbol{\omega}^\top (\mathbf{x} - \mathbf{x}')} d\mathbb{P}(\boldsymbol{\omega}), \quad (12)$$

where  $\mathbb{P}(\boldsymbol{\omega})$ , the Fourier dual of  $k$ , is equal to the *spectral density* of the kernel.  $\mathbb{P}(\boldsymbol{\omega})$  has all the properties of a cumulative distribution function except that  $\mathbb{P}(\infty) - \mathbb{P}(-\infty) = k(\mathbf{0})$  needs not to be equal to one [30]. However, in classic correlation functions such as the SE kernel  $\mathbb{P}(\boldsymbol{\omega})$  is a proper cumulative distribution function because  $k(\mathbf{0}) = 1$ . In this situation,  $p(\boldsymbol{\omega}) = \frac{d\mathbb{P}(\boldsymbol{\omega})}{d\boldsymbol{\omega}}$

is the density function of  $\omega$  and Equation (12) can be rewritten as

$$\begin{aligned} k(\mathbf{x}, \mathbf{x}') &= \int e^{-i\omega^\top(\mathbf{x}-\mathbf{x}')} p(\omega) d\omega = \mathbb{E}_{p(\omega)} [e^{-i\omega^\top(\mathbf{x}-\mathbf{x}')} ] \\ &= \mathbb{E}_{p(\omega)} [\operatorname{Re} (e^{-i\omega^\top \mathbf{x}} (e^{-i\omega^\top \mathbf{x}'})^*)] \\ &= \mathbb{E}_{p(\varphi)} [\varphi(\mathbf{x})^\top \varphi(\mathbf{x}')] . \end{aligned} \quad (13)$$

Here, the superscript  $*$  denotes the complex conjugate and  $\varphi(\cdot)$  is a random feature map. Note that there is no imaginary component in Equation (13) because we work with real-valued kernels. A possible choice for  $\varphi(\cdot)$  is

$$\varphi(\mathbf{x}) = \sqrt{2} \cos (\omega^\top \mathbf{x} + b) , \quad (14)$$

in which  $b \sim \mathcal{U}[0, 2\pi]$  is a uniform random variable [36, 22]. The distribution of  $\omega$  depends on the type of correlation function. For example, the spectral density  $p(\omega)$  of the Matérn kernel is a  $t$ -distribution and for the SE kernel is Gaussian specified by [36, 46]

$$\omega_{SE} \sim \mathcal{N}(\mathbf{0}, \Delta^{-1}) . \quad (15)$$

Now, we describe how the explicit random feature map  $\varphi(\mathbf{x})$  given by Equation (14) can be employed to approximate the stationary kernel  $k$ . To do this, first we need to take  $M$  independently and identically distributed (i.i.d.) samples from  $p(\omega)$  and  $p(b) = \mathcal{U}[0, 2\pi]$  using a Monte-Carlo approach. These samples are denoted by  $\omega^{(1)}, \dots, \omega^{(M)}$  and  $b^{(1)}, \dots, b^{(M)}$  by which the vector

$$\varphi(\mathbf{x}) = \sqrt{\frac{2}{M}} \left[ \cos (\omega^{(1)\top} \mathbf{x} + b^{(1)}) , \dots, \cos (\omega^{(M)\top} \mathbf{x} + b^{(M)}) \right]^\top , \quad (16)$$

is created. The map  $\varphi(\mathbf{x})$  transfers an input vector  $\mathbf{x}$  into an  $M$ -dimensional feature space. Finally, the correlation function  $k$  is approximated as below

$$k(\mathbf{x}, \mathbf{x}') = \mathbb{E}_{p(\varphi)} [\varphi(\mathbf{x})^\top \varphi(\mathbf{x}')] \approx \varphi(\mathbf{x})^\top \varphi(\mathbf{x}'). \quad (17)$$

### 3.2 GP prediction with random Fourier features

In the weight space representation of GPs, the (actual) feature map  $\phi(\mathbf{x})$ , which is possibly infinite dimensional, can be approximated by the  $M$ -dimensional random feature map  $\varphi(\mathbf{x})$  in Equation (16). This offers an estimation to the predictive mean (and variance) of  $Y(\mathbf{x})$  given by Equation (10) (and (11)). The approximated predictive mean takes the following form

$$\hat{\mu}_n(\mathbf{x}) = \mu_0(\mathbf{x}) + \varphi(\mathbf{x})^\top \left( \hat{\Phi} \hat{\Phi}^\top \right)^{-1} \hat{\Phi} (\mathbf{y} - \boldsymbol{\mu}) \quad (18)$$

---

**Algorithm 1** Approximating the predictive mean with RFF

---

Input: training set  $\{\mathbf{X}, \mathbf{y}\}$ , trend function  $\mu_0$ , kernel  $k$  and its spectral density  $p(\omega)$ ,  $M$ : dimension of random feature space

- 1: Draw  $M$  i.i.d. samples from  $p(\omega)$  and  $p(b) = \mathcal{U}[0, 2\pi]$
- 2: Construct  $\varphi(\mathbf{x})$  using Equation (16)
- 3: Compute  $\hat{\Phi} = [\varphi(\mathbf{x}^1), \dots, \varphi(\mathbf{x}^n)]$
- 4: Compute  $\hat{\mu}_n(\mathbf{x})$  using Equation (18)

---

wherein the  $M \times n$ -dimensional matrix  $\hat{\Phi} = [\varphi(\mathbf{x}^1), \dots, \varphi(\mathbf{x}^n)]$  provides an estimation to  $\Phi$ . The procedure to approximate the predictive mean with RFF is outlined in Algorithm 1.

Note that the expression in (18) is stochastic since the construction of  $\varphi(\mathbf{x})$  relies on i.i.d. samples taken from the kernel spectral density  $p(\omega)$  and  $p(b)$ , see Equation (16). As a result, one can draw multiple realisations from the approximated predictive mean by taking samples from  $p(\omega)$  and  $p(b)$  repeatedly. This idea is used in Section 4 for emulating dynamical simulators where multiple draws from the emulated flow map are employed to perform one-step ahead predictions. With this, one can quantify uncertainty of the time series prediction in the absence of a closed-form expression like Equation (11).

## 4 Emulating dynamical simulators

In this section, we introduce our methodology for emulating deterministic non-linear dynamical simulators that are computationally intensive. The method relies on predicting the numerical flow map over a short period using a GP whose kernel is approximated with RFF. Let  $\mathbf{x}(t_1) = (x_1(t_1), \dots, x_d(t_1))^\top$  denotes the solution of the system at  $t_1 = t_0 + \Delta t$  for a given fixed “small” time step  $\Delta t$  and initial condition  $\mathbf{x}_0$ . We assume that  $\mathbf{x}(t_1)$  is obtained by the flow map  $F$  defined as

$$F(\mathbf{x}_0) = (f_1(\mathbf{x}_0), \dots, f_d(\mathbf{x}_0))^\top = (x_1(t_1), \dots, x_d(t_1))^\top, \quad (19)$$

such that each map  $f_i : \mathcal{X} \mapsto \mathbb{R}$  yields the  $i$ -th component of  $\mathbf{x}(t_1)$ , i.e.  $x_i(t_1)$ . A prediction associated with the dynamics of  $x_i(t)$  is achieved by:

- Emulating  $f_i$  with a GP whose kernel is estimated with RFF
- Drawing a realisation from the approximated predictive mean of  $f_i$  based on Algorithm 1
- Using the realisation iteratively to perform one-step ahead predictions

It is desired to have an estimation of uncertainty associated with the time series prediction to assess the accuracy of the prediction. To this end,

we repeat the above steps with multiple draws from the emulated flow map to reach a probability distribution over the time series. The mean and variance of that distribution can serve as the model output prediction and the associated uncertainty, respectively. Our proposed emulation method is presented in Algorithm 2 where  $\hat{f}_i^{(s)}(\mathbf{x})$  indicates the  $s$ -th approximation to the predictive mean of the GP used to emulate  $f_i(\mathbf{x})$ .

The first step of Algorithm 2 is to choose  $n$  sample points  $\mathbf{X} = \{\mathbf{x}_0^1, \dots, \mathbf{x}_0^n\}$  from the space of initial conditions. These points are selected in a carefully designed experiment such that they fill the space uniformly. Such sampling strategy is called “space-filling” design and can be achieved via techniques such as Latin hypercube sampling (LHS) [19, 40]. The corresponding outputs are obtained by running the simulator at each  $\mathbf{x}_0^1, \dots, \mathbf{x}_0^n$  over the time horizon  $\Delta t$ .

---

**Algorithm 2** Emulating dynamic non-linear simulators

---

- 1: Select  $n$  space-filling initial conditions:  $\mathbf{X} = \{\mathbf{x}_0^1, \dots, \mathbf{x}_0^n\}$
- 2: Run the simulator for each  $\mathbf{x}_0^1, \dots, \mathbf{x}_0^n$  over  $\Delta t$  to obtain  
 $\mathbf{y} = \{\mathbf{x}^1(t_1), \dots, \mathbf{x}^n(t_1)\}$
- 3: **for**  $i = 1$  to  $d$  **do**
- 4:   Create  $\mathcal{D}_i = \{\mathbf{X}, \mathbf{y}_i\}$  where  $\mathbf{y}_i = (x_i^1(t_1), \dots, x_i^n(t_1))^{\top}$
- 5:   **for**  $s = 1$  to  $S$  **do**
- 6:     Generate  $\hat{f}_i^{(s)}(\mathbf{x})$  using Algorithm 1 and training set  $\mathcal{D}_i$
- 7:     Use  $\hat{f}_i^{(s)}(\mathbf{x})$  iteratively to perform one-step ahead predictions
- 8:   **end for**
- 9:   Calculate the mean and variance of the obtained time series
- 10: **end for**

---

## 5 Numerical results

The prediction performance of our proposed method is tested on several dynamic systems implemented as computer codes. They are the Lorenz [31], van der Pol [43] and Hindmarsh-Rose models [24]. These systems are further elaborated in the following subsections. The training data to emulate the short-time numerical flow map consists of  $n = 15 \times d$  points selected from the space of initial conditions. We use the `optimumLHS` function implemented in the R package `lhs` [9] to sample the initial conditions. This function maximises the mean distance between all candidate points, and hence yields a space-filling design. The GP correlation function is the squared exponential kernel which is recommended in [13, 34]. The kernel is approximated using RFF with  $M = 250$  as is considered in [22]. The number of realisations drawn from the emulated flow map is  $S = 100$ . The trend function is a first order polynomial regression whose coefficients are estimated via Equa-

tion (26). The length-scales and process variance are estimated by the ML method. The simulation time step is fixed and equal to  $\Delta t = 0.01$ . The ODEs are solved by the default solver of the package `deSolve` [42].

The accuracy of the time series prediction is measured via the *mean absolute error (MAE)* and *root mean square error (RMSE)* criteria. They are defined as

$$MAE = \frac{\sum_{t=1}^{t=T} |x(t) - \hat{x}(t)|}{n_{step}}, \quad (20)$$

$$RMSE = \sqrt{\frac{\sum_{t=1}^{t=T} (x(t) - \hat{x}(t))^2}{n_{step}}}, \quad (21)$$

in which  $T$  is the final time of the simulation and  $n_{step} = T/\Delta t$  denotes the total number of one-step ahead predictions. A criterion called the “predictability horizon” is suggested in [34] as the time after which the emulator is less reliable. It represents the time at which a change point occurs in the evolution of prediction uncertainties, see below for further details. The predictability horizon (denoted by  $t^*$ ) is computed for all test cases. Finally, we compare the results obtained by our method with the one presented in [34] which is also based on emulating the numerical flow map and one-step ahead predictions. We refer to our proposed approach as “Method 1” and the other one as “Method 2” in the rest of the paper.

## 5.1 Lorenz attractor

The Lorenz model is a system of ODE first derived by Edward Lorenz in 1963 [31]. Although the Lorenz system was originally developed as a model of convection in the earth’s atmosphere, it has applications to other fields, see e.g. [35]. The Lorenz system can produce a famous chaotic attractor whereby trajectories on the attractor are very sensitive to initial conditions. In other words, the evolution of the system starting from two slightly different points will be entirely dissimilar. An attractor is a bounded area in the state space such that the trajectories of all nearby points converge to it [45]. The Lorenz equations are expressed by

$$\begin{cases} \frac{dx_1}{dt} = a_1 x_1 + x_2 x_3 \\ \frac{dx_2}{dt} = a_2 (x_2 - x_3) \\ \frac{dx_3}{dt} = -x_1 x_2 + a_3 x_2 - x_3, \end{cases} \quad (22)$$

with the classic parameter values of  $a_1 = -8/3$ ,  $a_2 = -10$  and  $a_3 = 28$ . These values result in the well-known “butterfly attractor” as can be seen in Figure 1.

The emulation of the Lorenz model with Methods 1 and 2 is displayed in Figures 1 and 2, respectively. The parameters  $a_1$ ,  $a_2$  and  $a_3$  are set to the

values as above and the initial condition in both figures is  $\mathbf{x}_0 = (1, 1, 1)^\top$  displayed by a red point in the three-dimensional picture. It demonstrates the evolution of the state variables together. Throughout this paper, the simulation is shown in red and emulation in black; the credible intervals (= prediction  $\pm$  standard deviation of prediction) is shaded. The vertical dashed blue lines indicate the predictability horizon obtained by applying the `cpt.mean` function implemented in the `changepoint` R package [28] to the standard deviation (SD) of predictions. For example, Figure 3 illustrates the SD of predictions associated with the variables  $x_1$  and  $x_2$  in the Lorenz model. The change points (vertical lines) show the time at which a drastic change happens in the prediction uncertainties.

The two methods have similar performances in emulating the Lorenz system. The prediction accuracy is high up to about  $t \approx 14$ . After that time, the emulator deviates from the true model which has a chaotic behaviour and tends to the average of the process. At the same time, the prediction uncertainties blow which allows the credible intervals to encompass most values of the system. The MAE and RMSE criteria are computed for both approaches and presented together with the predictability horizon in Table 1. For each state variable, the first row is acquired using Method 1 and the second row with Method 2. The table also contains the results from emulating the Lorenz model with another initial condition, i.e.  $\mathbf{x}_0 = (-1, -1, -1)^\top$ . As can be seen, the values obtained by the two methods are close to each other suggesting that they are comparable.

Table 1: The MAE and RMSE criteria and predictability horizon of Method 1 (first row) and Method 2 (second row) obtained by two different initial conditions.

$\mathbf{x}_0 = (1, 1, 1)^\top$			$\mathbf{x}_0 = (-1, -1, -1)^\top$		
	MAE	RMSE		MAE	RMSE
$x_1$	3.34	5.46	13.68	2.43	5.06
	5.06	7.47	14.48	2.41	4.68
$x_2$	3.99	6.34	13.71	2.14	4.13
	3.97	6.14	14.44	2.30	4.45
$x_3$	4.32	7.20	13.65	2.34	4.71
	4.32	7.00	14.37	2.48	4.98

## 5.2 Van der Pol oscillator

The van der Pol equation was first proposed by the Dutch engineer Balthasar van der Pol in 1920 while working on the behaviour of vacuum tube circuits. Since then, this model has been extensively used to study oscillatory phenomena such as biological rhythms [47], heartbeat [18] and circadian

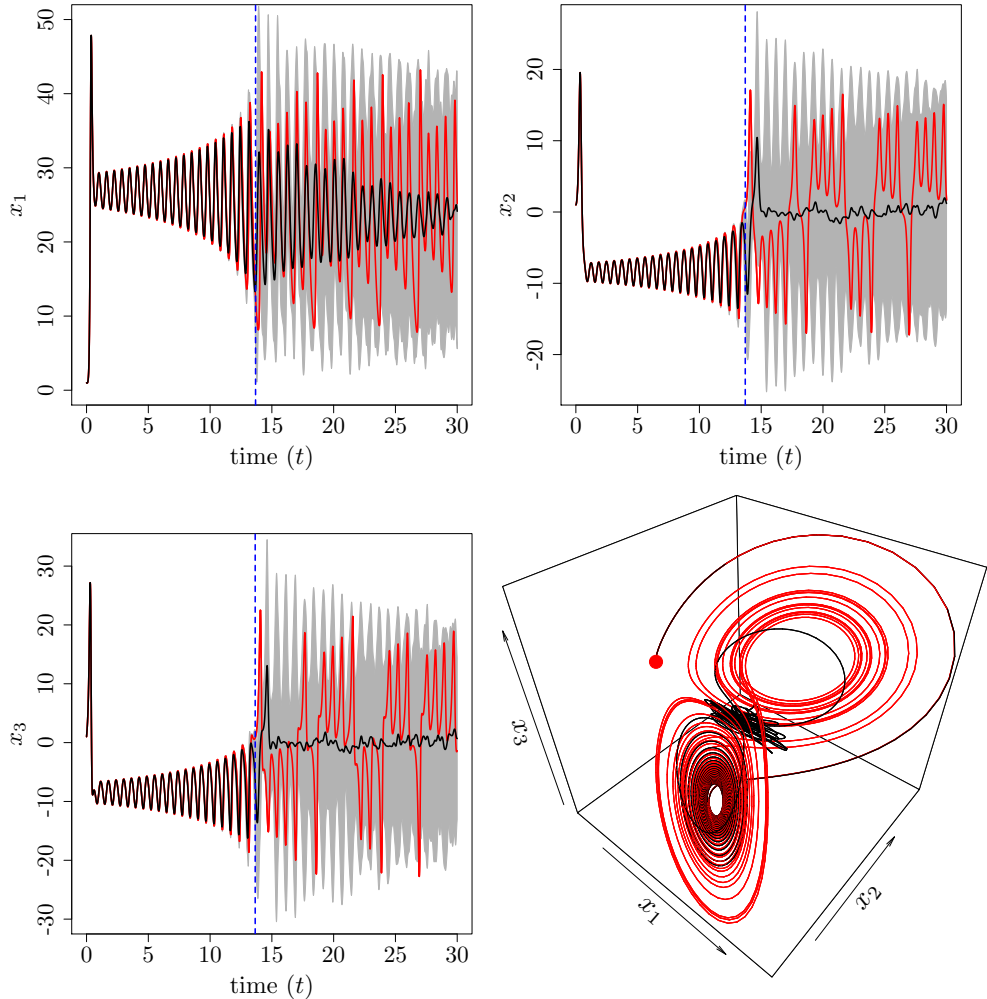


Figure 1: The prediction (black) and associated uncertainty (shaded) in emulating the Lorenz model (red) based on Method 1. The vertical dashed blue lines represent the predictability horizon which are the change point in the diagram of prediction uncertainties. The initial condition is  $\mathbf{x}_0 = (1, 1, 1)^\top$  which is shown by a red point in the three-dimensional picture. It shows the evolution of the whole system.

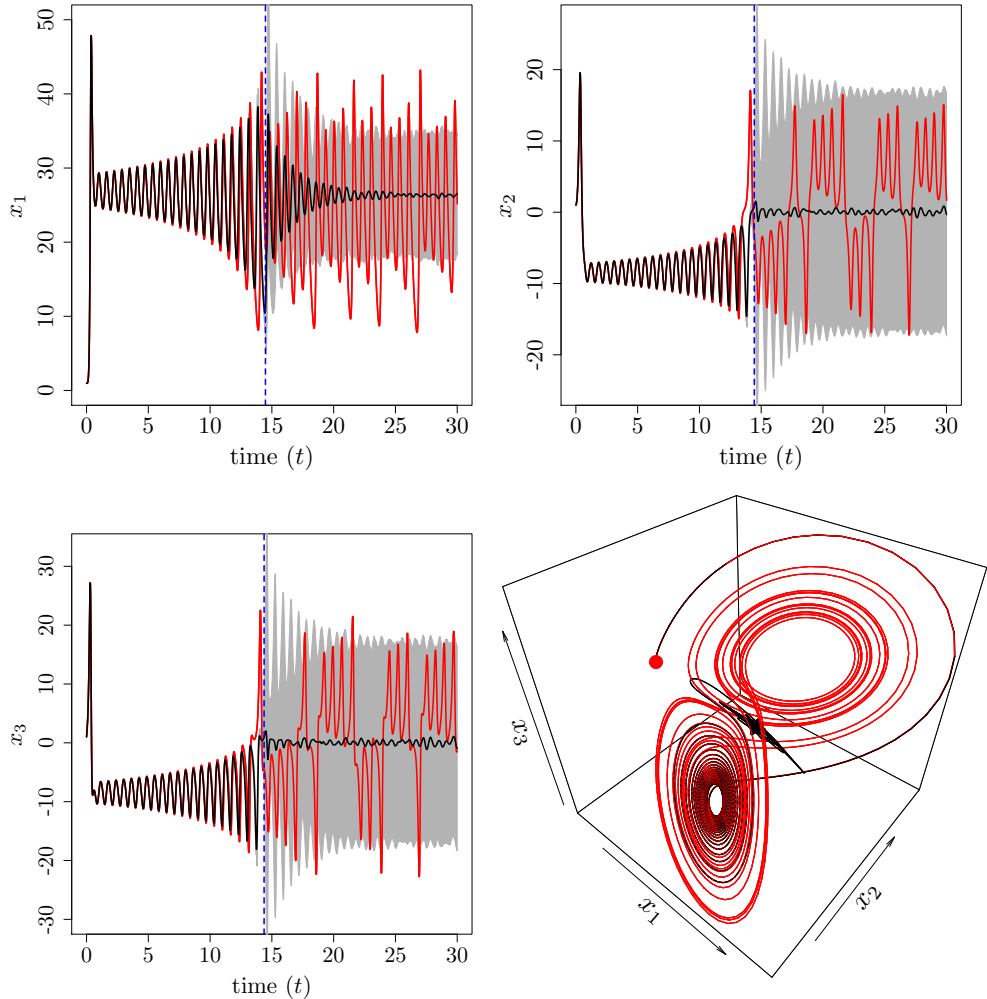


Figure 2: The Lorenz model (red) and its emulation (black) obtained by Method 2. The vertical dashed blue lines show the predictability horizon. The initial condition and the parameter values are the same as Figure 1.

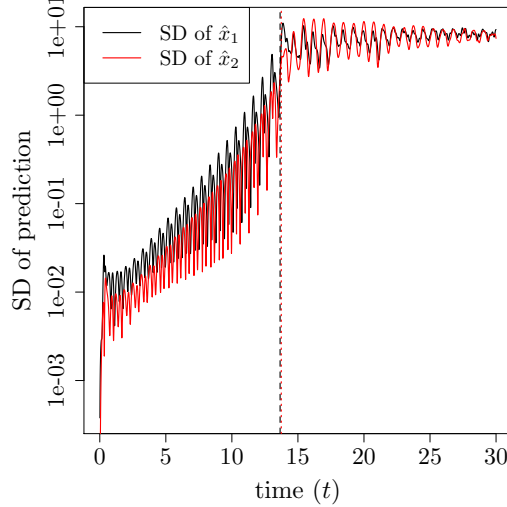


Figure 3: Standard deviation (SD) of prediction associated with the variables  $x_1$  (black) and  $x_2$  (red) in the Lorenz model. The vertical dashed lines show the change point of each diagram. The y-axis is on logarithmic scale.

rhythms [8]. The evolution of the van der Pol model in time is of the form [43]

$$\begin{cases} \frac{dx_1}{dt} = x_2 \\ \frac{dx_2}{dt} = a(1 - x_1^2)x_2 - x_1, \end{cases} \quad (23)$$

where the parameter  $a > 0$  controls the frequency of the oscillations. The van der Pol oscillator exhibits a periodic motion, i.e. a limit cycle, see Figure 4. The emulation of the van der Pol oscillator based on Methods 1 and 2 is visualised in Figures 4 and 5, respectively. The truth (red), prediction (black), credible intervals (shaded) and predictability horizon (dashed blue) are illustrated in the figures. The initial condition displayed by a red point in the two-dimensional picture is  $\mathbf{x}_0 = (1, 1)^\top$  and  $a = 5$  in both cases.

As can be seen, Method 1 outperforms Method 2 in emulating the van der Pol model. Specially, the first state variable is predicted with a high accuracy by Method 1 and the predictability horizon is equal to the total simulation time. There is a frequency miss-match in the predictions obtained by Method 2 after the predictability horizon. Moreover, the amplitude of the predictions (especially  $\hat{x}_2(t)$ ) in Method 2 gradually damps. However, this is a less severe problem in Method 1. The two methods are compared according to the MAE, RMSE and predictability horizon criteria. They are presented in Table 2 which also accommodates the measures obtained by an additional initial condition, i.e.  $\mathbf{x}_0 = (-1, -1)^\top$ . The criteria summarised in Table 2 suggest that Method 1 has a better prediction performance (especially in the case of the first state variable) than Method 2.

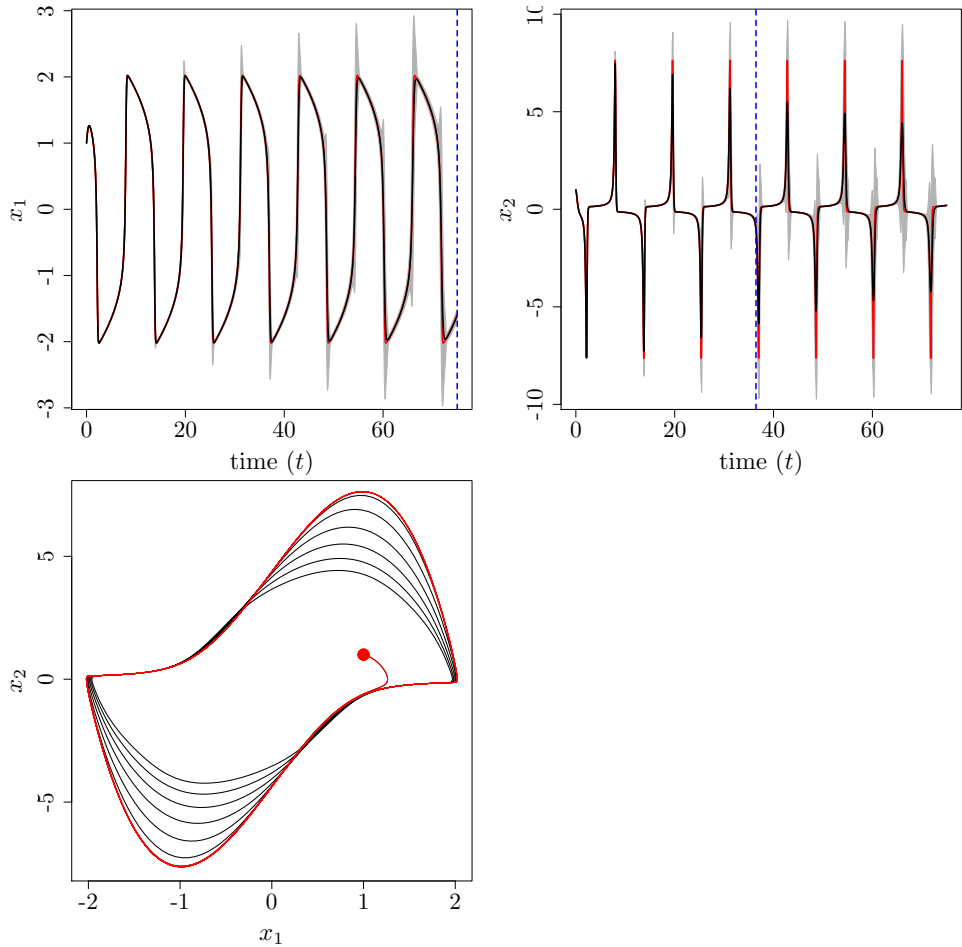


Figure 4: The van der Pol oscillator (red), the prediction (black) and credible intervals (shaded) using Method 1. The dashed blue lines show the predictability horizon. The initial condition (red point) and parameter value are  $\mathbf{x}_0 = (1, 1)^\top$  and  $a = 5$ .

Table 2: The MAE and RMSE criteria and predictability horizon obtained by Methods 1 and 2. For each variable, the first row consists of the criteria associated with Method 1 and the second row represents those of Method 2.

$\mathbf{x}_0 = (1, 1)^\top$			$\mathbf{x}_0 = (-1, -1)^\top$		
	MAE	RMSE	$t^*$	MAE	RMSE
$x_1$	0.02	0.07	75	0.03	0.08
	1.18	1.82	29.31	1.16	1.80
$x_2$	0.11	0.40	36.44	0.12	0.40
	0.83	1.67	24.73	0.83	1.67

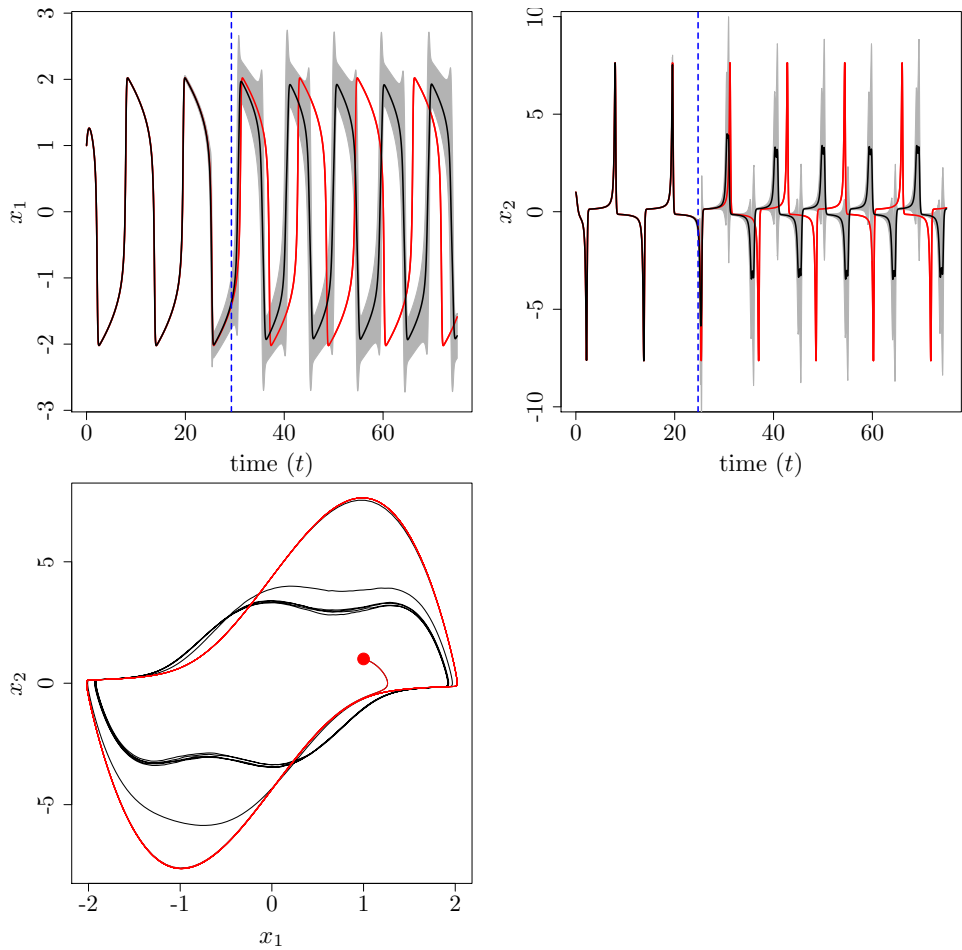


Figure 5: The van der Pol oscillator (red) and its emulation (black) using Method 2 where  $\mathbf{x}_0 = (1, 1)^\top$  and  $a = 5$ . The dashed blue lines are the predictability horizons. A frequency miss-match happens after the predictability horizon and the amplitude of the predictions gradually damp.

### 5.3 Hindmarsh-Rose model

The Hindmarsh-Rose (HR) model [24] is widely used in neuroscience to simulate the non-linear dynamics of a single neuron. Neurons are specialised cells that are responsible for generating electrical signals called *action potentials* by which information is transmitted throughout the nervous system. The HR model is capable of mimicking spiking and bursting which can be seen to occur in real cells. The mathematical equations of the HR model are

$$\begin{cases} \frac{dx_1}{dt} = x_2 - a_1 x_1^3 + a_2 x_1^2 - x_3 + I \\ \frac{dx_2}{dt} = a_3 - a_4 x_1^2 - x_2 \\ \frac{dx_3}{dt} = \varepsilon (a_5 (x_1 - x_{rest}) - x_3), \end{cases} \quad (24)$$

wherein  $x_1$  represents the cell membrane potential. The variables  $x_2$  and  $x_3$  describe the ionic currents flowing across the membrane through fast and slow ion channels, respectively. The parameter  $0 < \varepsilon \ll 1$  is small, which makes  $x_3$  a slow variable.  $I$  represents the membrane input current and  $x_{rest}$  is the rest potential of the system. Having studied a limit cycle and a chaotic behaviour, we then choose in the HR model a complex transient trajectory, where the two time scales interplay. The study of transient dynamics is important in many real-world phenomena, see e.g. [21, 29]. To this end, in our experiments the value of the parameters  $\varepsilon, I$  and  $x_{rest}$  are set to 0.01, 2.4 and -1.6, respectively. The constant parameters  $a_1, \dots, a_5$  are determined experimentally [15]; their typical values which are considered in the examples below are:  $a_1 = 1, a_2 = 2.7, a_3 = 1, a_4 = 5$  and  $a_5 = 4$  [3].

Figures 6 and 7 present the HR model (red) and its emulation (black) based on Methods 1 and 2, respectively. In both figures, the initial condition is  $\mathbf{x}_0 = (1, 1, 1)^\top$ . As can be seen, Method 1 has a superior performance compared to Method 2 in forecasting all three variables. Particularly, in Method 1 the emulator remains reliable until the end of simulation and the predictability horizon is equal to:  $t^* = 100$ . Methods 1 and 2 are compared according to the MAE, RMSE and predictability horizon criteria in Table 3 with an extra initial condition  $\mathbf{x}_0 = (-1, -1, -1)^\top$ . The criteria obtained by Method 1 are clearly better than those of Method 2. It can be seen that the values of MAE and RMSE in Methods 1 do not usually exceed 0.07, indicating a high prediction accuracy.

## 6 Conclusions

This paper proposes a novel approach for emulating computationally expensive dynamic computer codes whose output is a time series. The method is based on approximating the short-time numerical flow map and using the emulated flow map in an iterative manner to perform one-step ahead predictions. The flow map is a function that gives the solution of a dynamic system

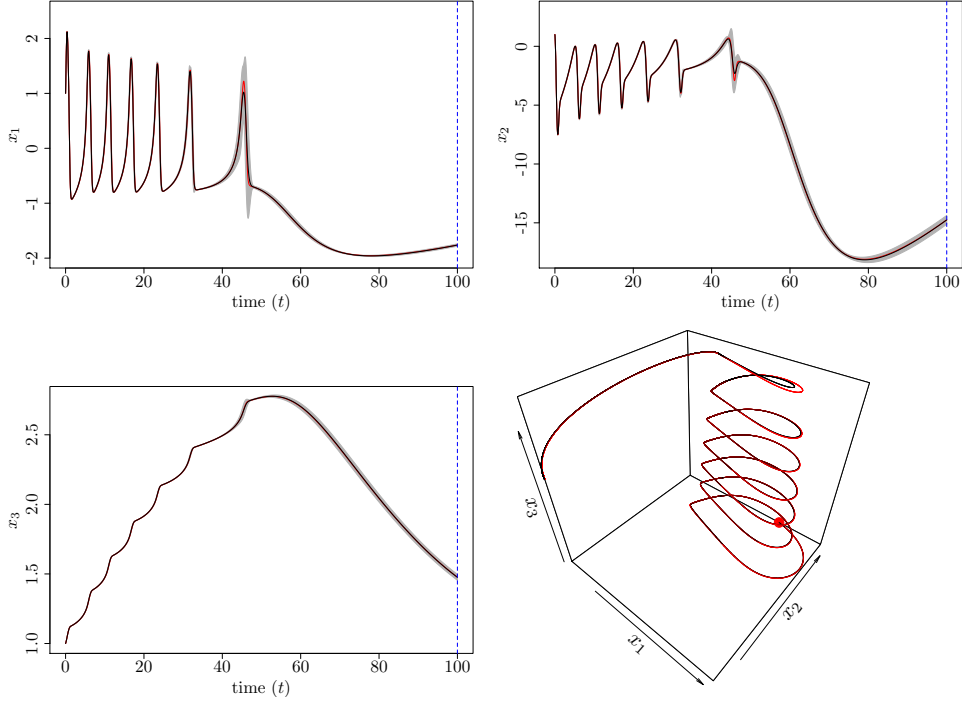


Figure 6: Emulating the HR model with the initial condition  $\mathbf{x}_0 = (1, 1, 1)^\top$  based on Method 1. The proposed approach has a high prediction performance such that the difference between the truth (red) and emulation (black) is negligible. The predictability horizon (dashed blue) occurs at the end of the simulation for all three variables.

Table 3: Comparison of Methods 1 and 2 in emulating the HR model. For each variable, the predictive performance of Methods 1 and 2 is presented in the first and the second row, respectively.

$\mathbf{x}_0 = (1, 1, 1)^\top$			$\mathbf{x}_0 = (-1, -1, -1)^\top$			
	MAE	RMSE		MAE	RMSE	
$x_1$	0.01	0.03	100	0.02	0.04	79.53
	0.48	0.64	71.18	0.45	0.61	28.58
$x_2$	0.04	0.07	100	0.16	0.34	81.91
	3.45	5.10	16.19	1.46	2.02	29.08
$x_3$	0.001	0.002	100	0.008	0.02	100
	0.54	0.71	100	0.35	0.50	100

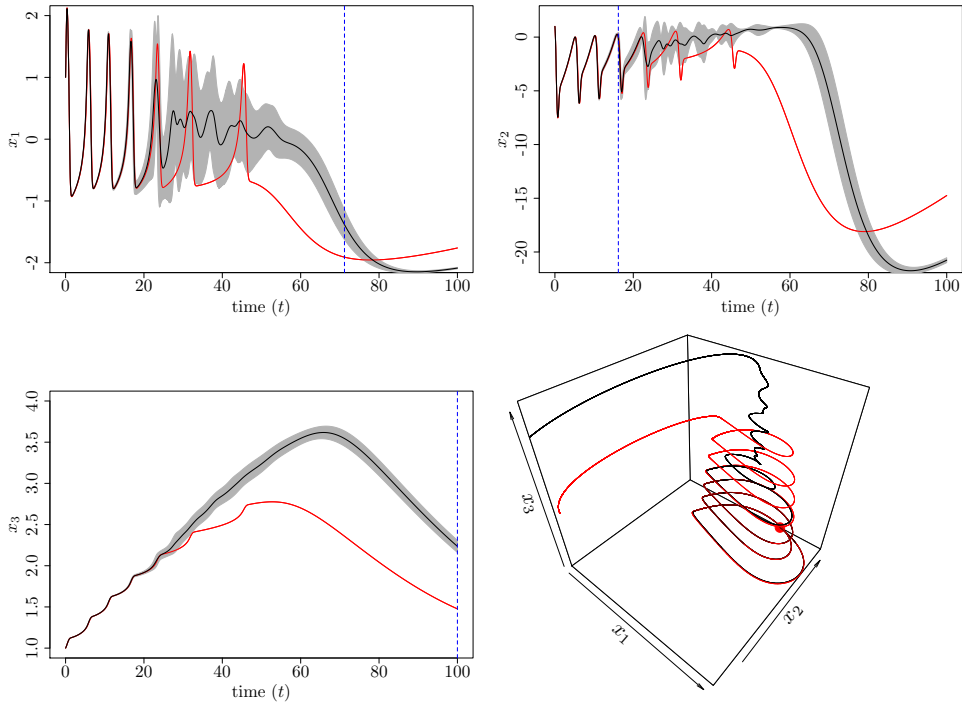


Figure 7: Emulating the HR model with the initial condition  $\mathbf{x}_0 = (1, 1, 1)^\top$  using Method 2. The simulation and emulation are shown in red and black, respectively. This approach has a lower prediction performance compared to Method 1, see Figure 6.

at an arbitrary time for a given initial condition. The main contribution of this paper is that the flow map function is emulated by a GP whose kernel is estimated using RFF. This allows us to draw multiple realisations from the emulated flow map. When the realisations are employed in the one-step ahead prediction paradigm, a distribution over the time series is created. The mean and variance of that distribution serve as the prediction and a measure of the associated uncertainty, respectively. The proposed method is tested on several non-linear dynamic simulators including the Lorenz attractor and van der Pol oscillator. The results suggest that our approach can emulate those models precisely with an accurate representation of the prediction uncertainty.

## Acknowledgments

The authors (HM and PC) would like to thank the Alan Turing Institute for funding this work.

## Appendix A Parameter estimation

The stochastic process  $Y(\mathbf{x})$  depends on a set of hyperparameters  $\boldsymbol{\theta}$  that are generally unknown and need to be estimated from the data. Suppose that  $\boldsymbol{\theta} = \{\sigma_0^2, \boldsymbol{\beta}, \boldsymbol{\delta}\}$  is the set of hyperparameters where  $\boldsymbol{\delta} = [\delta_1, \dots, \delta_d]^\top$ . We use the maximum likelihood method to estimate them. The logarithm of the likelihood function is

$$\mathcal{L}(\boldsymbol{\theta} \mid \mathbf{y}) = -\frac{n}{2} \ln(2\pi\sigma_0^2) - \frac{1}{2} \ln(|\mathbf{K}|) - \frac{1}{2\sigma_0^2} (\mathbf{y} - \boldsymbol{\mu})^\top \mathbf{K}^{-1} (\mathbf{y} - \boldsymbol{\mu}), \quad (25)$$

where the correlation matrix  $\mathbf{K}$  depends on  $\boldsymbol{\delta}$  and  $\boldsymbol{\mu} = \mathbf{Q}\boldsymbol{\beta}$  in which  $\mathbf{Q} = [\mathbf{q}(\mathbf{x}^1), \dots, \mathbf{q}(\mathbf{x}^n)]^\top$ . It is an  $n \times r$  matrix called the *experimental matrix* and comprises the evaluation of the regression functions at the training data. An estimate of  $\boldsymbol{\beta}$  and  $\sigma_0^2$  is obtained by taking the derivatives of  $\mathcal{L}(\boldsymbol{\theta} \mid \mathbf{y})$  with respect to those parameters and setting the derivatives to zero. The estimated parameters have closed-form expressions given by

$$\hat{\boldsymbol{\beta}} = (\mathbf{Q}^\top \mathbf{K}^{-1} \mathbf{Q})^{-1} \mathbf{Q}^\top \mathbf{K}^{-1} \mathbf{y}, \quad (26)$$

$$\hat{\sigma}_0^2 = \frac{1}{n} (\mathbf{y} - \mathbf{Q}\hat{\boldsymbol{\beta}})^\top \mathbf{K}^{-1} (\mathbf{y} - \mathbf{Q}\hat{\boldsymbol{\beta}}). \quad (27)$$

If the parameters  $\boldsymbol{\beta}$  and  $\sigma_0^2$  in Equation (25) are substituted with their estimates  $\hat{\boldsymbol{\beta}}$  and  $\hat{\sigma}_0^2$ , the profile log-likelihood (after dropping the constants) is achieved as

$$\mathcal{L}_p(\boldsymbol{\delta} \mid \mathbf{y}) = -\frac{n}{2} \ln(\hat{\sigma}_0^2) - \frac{1}{2} \ln(|\mathbf{K}|). \quad (28)$$

Finally, the length-scales can be estimated by solving the optimisation problem below

$$\hat{\boldsymbol{\delta}} = \arg \max_{\boldsymbol{\delta}} \mathcal{L}_p(\boldsymbol{\delta} \mid \mathbf{y}). \quad (29)$$

## References

- [1] Mauricio A. Álvarez and Neil D. Lawrence. Computationally efficient convolved multiple output Gaussian processes. *Journal of Machine Learning Research*, 12(41):1459–1500, 2011.
- [2] N. Aronszajn. Theory of reproducing kernels. *Transactions of the American Mathematical Society*, 68(3):337–404, 1950.
- [3] Roberto Barrio and Andrey Shilnikov. Parameter-sweeping techniques for temporal dynamics of neuronal systems: Case study of hindmarsh-rose model. *Journal of mathematical neuroscience*, 1:6, 2011.
- [4] M. J. Bayarri, J. O. Berger, J. Cafeo, G. Garcia-Donato, F. Liu, J. Palomo, R. J. Parthasarathy, R. Paulo, J. Sacks, and D. Walsh. Computer model validation with functional output. *The Annals of Statistics*, 35(5):1874–1906, 2007.
- [5] Sourabh Bhattacharya. A simulation approach to Bayesian emulation of complex dynamic computer models. *Bayesian Analysis*, 2(4):783–815, 2007.
- [6] Salomon Bochner. *Lectures on Fourier Integrals*. Princeton University Press, 1959.
- [7] S.L. Brunton and J.N. Kutz. *Data-Driven Science and Engineering: Machine Learning, Dynamical Systems, and Control*. Cambridge University Press, 2019.
- [8] Erika Camacho, Richard Rand, and Howard Howland. Dynamics of two van der Pol oscillators coupled via a bath. *International Journal of Solids and Structures*, 41(8):2133–2143, 2004.
- [9] Rob Carnell. *lhs: Latin Hypercube Samples*, 2020. R package version 1.1.1.
- [10] A. Castelletti, S. Galelli, M. Ratto, R. Soncini-Sessa, and P.C. Young. A general framework for dynamic emulation modelling in environmental problems. *Environmental Modelling & Software*, 34:5 – 18, 2012.

- [11] Ricky T. Q. Chen, Yulia Rubanova, Jesse Bettencourt, and David K Duvenaud. Neural ordinary differential equations. In *Advances in Neural Information Processing Systems 31*, pages 6571–6583. 2018.
- [12] Victoria C. P. Chen, Kwok-Leung Tsui, Russell R. Barton, and Martin Meckesheimer. A review on design, modeling and applications of computer experiments. *IIE Transactions*, 38(4):273–291, 2006.
- [13] S. Conti, J. P. Gosling, J. E. Oakley, and A. O’Hagan. Gaussian process emulation of dynamic computer codes. *Biometrika*, 96:663–676, 2009.
- [14] Steo Conti and Anthony O’Hagan. Bayesian emulation of complex multi-output and dynamic computer models. *Journal of Statistical Planning and Inference*, 140(3):640–651, 2010.
- [15] Nathalie Corson and Moulay Aziz-Alaoui. Asymptotic dynamics of Hindmarsh-Rose neuronal system. *Dynamics of Continuous, Discrete and Impulsive Systems, Series B: Applications and Algorithms*, (16):535–549, 2009.
- [16] P. Cvitanović, R. Artuso, R. Mainieri, G. Tanner, and G. Vattay. *Chaos: Classical and Quantum*. Niels Bohr Institute, Copenhagen, 2016.
- [17] F. Dernoncourt, K. Veeramachaneni, and U. M. O’Reilly. Gaussian process-based feature selection for wavelet parameters: Predicting acute hypotensive episodes from physiological signals. In *2015 IEEE 28th International Symposium on Computer-Based Medical Systems*, pages 145–150, 2015.
- [18] Angela M. dos Santos, Sergio R. Lopes, and R.L.Ricardo L. Viana. Rhythm synchronization and chaotic modulation of coupled van der Pol oscillators in a model for the heartbeat. *Physica A: Statistical Mechanics and its Applications*, 338(3):335–355, 2004.
- [19] Kai-Tai Fang, Dennis K. J. Lin, Peter Winker, and Yong Zhang. Uniform design: Theory and application. *Technometrics*, 42(3):237–248, 2000.
- [20] Thomas E. Fricker, Jeremy E. Oakley, and Nathan M. Urban. Multivariate Gaussian process emulators with nonseparable covariance structures. *Technometrics*, 55(1):47–56, 2013.
- [21] Marc Goodfellow, Kaspar Schindler, and Gerold Baier. Self-organised transients in a neural mass model of epileptogenic tissue dynamics. *NeuroImage*, 59(3):2644–2660, 2012.

- [22] José Miguel Henández-Lobato, Matthew W. Hoffman, and Zoubin Ghahramani. Predictive entropy search for efficient global optimization of black-box functions. In *Proceedings of the 27th International Conference on Neural Information Processing Systems*, NIPS’14, pages 918–926. MIT Press, 2014.
- [23] Dave Higdon, James Gattiker, Brian Williams, and Maria Rightley. Computer model calibration using high-dimensional output. *Journal of the American Statistical Association*, 103(482):570–583, 2008.
- [24] J. L. Hindmarsh and R. M. Rose. A model of neuronal bursting using three coupled first order differential equations. *Proceedings of the Royal Society of London*, 221(1222):87–102, 1984.
- [25] Thomas Hofmann, Bernhard Schölkopf, and Alexander J. Smola. Kernel methods in machine learning. *Annals of Statistics*, 36(3):1171–1220, 2008.
- [26] Gaofeng Jia and Alexandros A. Taflanidis. Kriging metamodeling for approximation of high-dimensional wave and surge responses in real-time storm/hurricane risk assessment. *Computer Methods in Applied Mechanics and Engineering*, 261-262:24–38, 2013.
- [27] Marc C. Kennedy and Anthony O’Hagan. Bayesian calibration of computer models. *Journal of the Royal Statistical Society: Series B (Statistical Methodology)*, 63(3):425–464, 2001.
- [28] Rebecca Killick and Idris Eckley. changepoint: An R Package for Changepoint Analysis. *Journal of Statistical Software*, 58(3):1–19, 2014.
- [29] Tim Kittel, Jobst Heitzig, Kevin Webster, and Jürgen Kurths. Timing of transients: quantifying reaching times and transient behavior in complex systems. *New Journal of Physics*, 19(8):083005, 2017.
- [30] Georg Lindgren. *Lectures on stationary stochastic processes*. Lund University Press, 2006.
- [31] Edward N. Lorenz. Deterministic nonperiodic flow. *Journal of Atmospheric Sciences*, 20:130–148, 1963.
- [32] David Machac, Peter Reichert, and Carlo Albert. Emulation of dynamic simulators with application to hydrology. *Journal of Computational Physics*, 313:352–366, 2016.
- [33] Colleen C. Mitchell and David G. Schaeffer. A two-current model for the dynamics of cardiac membrane. *Bulletin of Mathematical Biology*, 65(5):767–793, 2003.

- [34] Hossein Mohammadi, Peter Challenor, and Marc Goodfellow. Emulating dynamic non-linear simulators using Gaussian processes. *Computational Statistics & Data Analysis*, 139:178–196, 2019.
- [35] Edgar E. Peters. A chaotic attractor for the s&p 500. *Financial Analysts Journal*, 47(2):55–62, 1991.
- [36] Ali Rahimi and Benjamin Recht. Random features for large-scale kernel machines. In *Advances in Neural Information Processing Systems*, pages 1177–1184. 2008.
- [37] M. Raissi, P. Perdikaris, and G.E. Karniadakis. Physics-informed neural networks: A deep learning framework for solving forward and inverse problems involving nonlinear partial differential equations. *Journal of Computational Physics*, 378:686–707, 2019.
- [38] Carl Edward Rasmussen and Christopher K. I. Williams. *Gaussian processes for machine learning (adaptive computation and machine learning)*. The MIT Press, 2005.
- [39] Jerome Sacks, William J. Welch, Toby J. Mitchell, and Henry P. Wynn. Design and analysis of computer experiments. *Statistical Science*, 4(4):409–423, 1989.
- [40] T. J. Santner, Williams B., and Notz W. *The design and analysis of computer experiments*. Springer-Verlag, 2003.
- [41] Bernhard Scholkopf and Alexander J. Smola. *Learning with kernels: Support vector machines, regularization, optimization, and beyond*. MIT Press, Cambridge, MA, USA, 2001.
- [42] Karline Soetaert, Thomas Petzoldt, and R. Woodrow Setzer. Solving differential equations in R: Package deSolve. *Journal of Statistical Software*, 33(9):1–25, 2010.
- [43] S.H. Strogatz. *Nonlinear dynamics and chaos*. Studies in nonlinearity. Sarat Book House, 2007.
- [44] Mark van der Wilk. *Sparse Gaussian process approximations and applications*. PhD thesis, University of Cambridge, 2019.
- [45] Marcelo Viana. What’s new on lorenz strange attractors? *The Mathematical Intelligencer*, 22:6–19, 2000.
- [46] Ziyu Wang. *Practical and theoretical advances in Bayesian optimization*. PhD thesis, University of Oxford, 2016.
- [47] Arthur T. Winfree. Biological rhythms and the behavior of populations of coupled oscillators. *Journal of Theoretical Biology*, 16(1):15–42, 1967.

[48] Kirsten Zickfeld, Slawig Thomas, and Stefan Rahmstorf. A low-order model for the response of the atlantic thermohaline circulation to climate change. *Ocean Dynamics*, 54:8–26, 2004.